Applied Catalysis B: Environmental 94 (2010) 158–165

Contents lists available at ScienceDirect

Applied Catalysis B: Environmental

journal homepage: www.elsevier.com/locate/apcatb

# Novel preparation of nanosized mesoporous $SnO_2$ powders: Physicochemical and catalytic properties

Momtchil Dimitrov [a,b,*], Tanya Tsoncheva [a], Shaofeng Shao [b], Ralf Köhn [b,1]

[a] Institute of Organic Chemistry with Centre of Phytochemistry, Bulgarian Academy of Sciences, Sofia, Bulgaria
[b] Ludwig-Maximilian University, Department of Chemistry and Biochemistry, Munich, Germany

ARTICLE INFO

*Article history:*
Received 22 July 2009
Received in revised form 30 October 2009
Accepted 7 November 2009
Available online 13 November 2009

*Keywords:*
Nanocrystallites
Mesoporous
$SnO_2$
Oxidation
Catalysis

ABSTRACT

Two series of catalytically active $SnO_2$ powders were prepared from tin(IV) *tert*-butoxide and tin(IV) chloride as tin precursors. A part of the synthesized samples were additionally subjected to specific treatments during the preparation—a treatment at constant humidity and temperature and/or a "step calcination". The obtained samples were characterized by powder X-ray diffraction, nitrogen physisorption, transmission electron microscopy and were studied in the total oxidation of ethyl acetate. The use of these specific treatments leads to materials that differ substantially in their textural characteristics and catalytic properties. The highest catalytic activity and selectivity are obtained for samples prepared from tin(IV) *tert*-butoxide after the "step calcination" treatment.



## 1. Introduction

Size and shape of particles, their crystallinity and surface characteristics highly depend on the route of synthesis and post-synthetic treatments for a given material. Hence, a brief description of the preparation pathway is no longer satisfactory and can cause significant problems with respect to the materials properties and reproducibility. There exists an urge to know the basic physicochemical processes that occur during the formation of the nanoparticles. This would be very helpful for establishing the mechanisms of particle formation and would also be of importance in controlling the final properties of the obtained material. Therefore the synthesis of nanoparticles has become a highly developed field and attracted the attention of the scientists in their pursuit of structural peculiarities and various unusual physical, chemical and catalytic properties [1–6].

On the other hand, catalytic oxidation reactions have been extensively investigated in the past few years [7–13]. There has been an increasing interest connected to environmental and health concerns arising from pollution caused by volatile organic compounds (VOCs) emitted from various industries and automobile exhausts [9–13]. A major source of VOC emissions is the use of solvents and solvent containing products. In the last decades the catalytic combustion of VOCs was widely used for air pollution control, but still more effective and stable catalysts are needed especially for automotive applications. A major problem within this context is the selectivity to complete the VOCs oxidation as the reaction intermediates are sometimes more toxic than the original compounds [11,13]. In this aspect, ethyl acetate is a suitable model VOC representative because it represents one of the main and hard to oxidize pollutants in printing industry.

The oxidation of organic molecules by metal oxides usually proceeds by the Mars–van Krevelen mechanism [14,15]. The molecule is oxidized by the catalyst which is then reoxidized by gasphase oxygen. Thus, the catalyst must be characterized by a facile change of the oxidation state of its surface cations. As a great number of metal oxides can change the electronic states of metals in a wide range they are components of all active and selective catalysts and can be used as active catalytic supports as well. It has been pointed out that the participation of the lattice oxide ions into the catalytic oxidation demands a rapid migration of oxide ions in the bulk of the catalyst. This strongly depends on the defect structure of the bulk oxide catalyst [16]. Tin dioxide represents such a defect structure. It comprises large numbers of crystal defects that ensure high mobility of lattice oxygen. Besides, its instrinsic non-stoichiometry could be used more efficiently if the $SnO_2$ particle size is decreased due to faster migration of the oxide

* Corresponding author at: Institute of Organic Chemistry with Centre of Phytochemistry, Bulgarian Academy of Sciences, Acad. G. Bonchev Str., Bl. 9, 1113 Sofia, Bulgaria. Tel.: +359 2 9606111; fax: +359 2 8700225.
*E-mail addresses:* md2@orgchm.bas.bg, md2@abv.bg (M. Dimitrov), ralf.koehn@cup.uni-muenchen.de (R. Köhn).
[1] Address: Department of Chemistry & Biochemistry, University of Munich, Butenandtstraße 11, 82377 Munich, Germany. Tel.: +49 0 89 218077808; fax: +49 0 89 218077622.

0926-3373/$ – see front matter © 2009 Elsevier B.V. All rights reserved.
doi:10.1016/j.apcatb.2009.11.004

ions within the $SnO_2$ nanoparticles to lattice positions and also the more likely higher exposure of defects due to increased surface to volume ratio. Additionally, the presence of uniform mesopore system usually results in facilitated transport of reagents and products in a given catalytic reaction [17]. This way an unique type of active supports could be prepared due to particle miniaturization in the nanometer range Nanoparticles of tin dioxide have been synthesized by various chemical routes, e.g. precipitation [18,19], sol–gel [20,21], hydrothermal [21,22], micro-wave assisted syntheses [23], and ultrasonic spray pyrolysis [24]. Allthough the development of agglomerates should be avoided, their growing is somehow inevitable due to the small diameter of the particles and due to the presence of other compounds involved in these procedures, mainly solvents. On the other hand, the most used tin precursors are tin chlorides ($SnCl_2$ or $SnCl_4$) due to their low cost and easy handling. However, the chlorine ion is difficult to remove from the system and it seriously alters the final characteristics of the obtained materials, favoring the agglomeration of the particles [25] and thus reducing their catalytic behavior. This problem can be avoided by the use of organic tin precursors such as alkoxides.

A very interesting procedure has been used for increasing the specific surface area of $SnO_2$ thin films by means of reorganization of the $SnO_2$ species before calcination, leading to a structural "disorder to order" transition [26,27]. It represents a post-synthetic thermal vapor treatment at constant temperature and humidity, referred to as "delayed humidity treatment" (DHT), performed at a stage in the synthesis before significant hydrolysis and condensation processes or aging had taken place within the as-synthesized $SnO_2$ thin films. However, up to now it has not been performed for powder materials.

The present paper deals with the comparison of the properties of $SnO_2$ powders prepared by sol–gel techniques from Sn(IV) *tert*-butoxide and $SnCl_4$ as tin sources. The influence of the used specific post-synthetic treatments (DHT and "step calcination") on the final textural characteristics and catalytic properties of the obtained powder samples has been thoroughly investigated. The treatments lead to low-temperature particle crystallization and to a substantial increase in the specific surface area and pore volume and thus make these materials very promising active catalytic supports and furthermore active and stable oxidation catalysts.

## 2. Experimental

### 2.1. Materials

Tin(IV) *tert*-butoxide was used as tin precursor for the sample series A prepared by a sol–gel approach according to the literature [28,29]. The as-prepared solutions were spin-coated on watch glasses starting from 70 to 700 rpm. The relative humidity was regulated in the range of 10–15% during spin-coating. All samples were stored overnight in a closed environment (glove bag) for aging; afterwards some of them were subjected for 24 h to a specific treatment (DHT) under 70% humidity, using a saturated $NH_4NO_3$ aqueous solution in a closed desiccator at 343 K. Prior to caclination the powders were scrached of the watch glasses. Two different calcination procedures were applied to achieve the final $SnO_2$ materials: (i) a standard calcination procedure with a temperature increase of 1 K/min up to 673 K and dwelling times of 6 h at 373 K, 2 h at 473 K and 5 h at 673 K; (ii) a so-called "step calcination" (SC) with temperature increase of 0.25 K/min up to 573 K and dwelling times of 2 h at 373, 398, 423, 448, 473, 498, 523 and 573 K, and further temperature increase of 1 K/min to 673 K and a residence time of 5 h. The obtained samples are designated with the formulae: $A_i - (j)T$, where $i$ is either P or F accounting for the surfactant (Pluronic P123 or Pluronic F127, respectively) if present during synthesis, $j$ stands for the type of specific treatment used during sample preparation (DHT, "step calcination", or combination of both), and $T$ gives the final temperature of the specific treatment used in case of the intermediate samples (see Table 1).

The second sample series B was prepared using $SnCl_4$ as tin precursor according to the following synthesis procedure: 3 g of $SnCl_4$ were added to a solution of 4.15 g distilled water, 26.53 g EtOH and 1.45 g Pluronic F127 (or Pluronic P123) as surfactants. Sols with the following molar compositions were obtained:

1.0 $SnCl_4$:0.01 F127 (P123):50 EtOH:20 $H_2O$ and
1.0 $SnCl_4$:50 EtOH:20 $H_2O$—for the sample without surfactant.

The as-prepared sols were stirred at room temperature for 4 h and then the solvent was removed in a rotary evaporator. The

**Table 1**
Physicochemical characteristics of the investigated samples.

| Sample | Sn precursor | Surfactant | Treatment | BET[a] ($m^2$/g) | $d_{pore}$[b] (nm) | $V_{tot}$[c] (cc/g) | $D$[d] (nm) |
|---|---|---|---|---|---|---|---|
| *Pure tin oxides* | | | | | | | |
| A | $Sn(OC(CH_3)_3)_4$ | – | 673 K | 74 | 4.3 | 0.06 | 5.0 |
| A-(DHT) | $Sn(OC(CH_3)_3)_4$ | – | DHT + 673 K | 99 | 4.3 | 0.09 | 5.5 |
| B | $SnCl_4$ | – | 673 K | 52 | – | 0.37 | 9.9 |
| *Tin oxides with P123 from tin(IV) tert-butoxide (Intermediates)* | | | | | | | |
| $A_P$-(DHT)343 | $Sn(OC(CH_3)_3)_4$ | P123 | DHT 343 K | – | – | – | 2.2 |
| $A_P$-(DHT + SC)498 | $Sn(OC(CH_3)_3)_4$ | P123 | DHT + SC 498 K | 332 | 5.4 | 0.39 | 2.8 |
| $A_P$-(SC)498 | $Sn(OC(CH_3)_3)_4$ | P123 | SC 498 K | 406 | 3.3 | 0.36 | – |
| $A_P$-(SC)573 | $Sn(OC(CH_3)_3)_4$ | P123 | SC 573 K | 207 | 4.3 | 0.22 | 2.6 |
| *Tin oxides with P123 from tin(IV) tert-butoxide* | | | | | | | |
| $A_P$ | $Sn(OC(CH_3)_3)_4$ | P123 | 673 K | 85 | 5.1; 8.7 | 0.09 | 4.8 |
| $A_P$-(SC) | $Sn(OC(CH_3)_3)_4$ | P123 | sc 673 K | 107 | 6.3; 16.3 | 0.23 | 4.2 |
| $A_P$-(DHT) | $Sn(OC(CH_3)_3)_4$ | P123 | DHT + 673 K | 120 | 8.5 | 0.31 | 6.2 |
| $A_P$-(DHT_SC) | $Sn(OC(CH_3)_3)_4$ | P123 | DHT + sc 673 K | 103 | 9.8 | 0.30 | 5.5 |
| *Tin oxides with P123 from tin chloride* | | | | | | | |
| $B_P$ | $SnCl_4$ | P123 | 673 K | 66 | 6.3 | 0.10 | 11.7 |
| $B_P$-(DHT) | $SnCl_4$ | P123 | DHT + 673 K | 71 | 6.4 | 0.11 | 11.2 |
| $B_F$ | $SnCl_4$ | F127 | 673 K | 83 | 7.5 | 0.16 | 7.0 |
| $B_F$-(DHT) | $SnCl_4$ | F127 | DHT + 673 K | 88 | 6.8 | 0.16 | 7.3 |

[a] BET specific surface area.
[b] Main pore diameter evaluated from NLDFT pore size distribution curves—half-width at half maximum.
[c] Total pore volume.
[d] Average particle size calculated with the Scherrer equation.

obtained powders were dried overnight in vacuum; some of them were subjected to DHT before being calcined using the standard calcination procedure (see above). The samples from this series were designated as B, $B_F$, $B_F$-(DHT), $B_P$ and $B_P$-(DHT) (see Table 1).

### 2.2. Methods and apparatus

The crystallinity of the samples was investigated by powder X-ray diffraction (PXRD) measurements performed on a Scintag XGEN-400 and a Stoe powder diffractometer in reflection or transmission geometry using Cu Kα sources. The size of the crystalline domains in the samples was determined based on the Scherrer equation [30], using the line broadening of the 1 1 0 Bragg reflection (the fitting of the diffraction patterns was carried out with Lorentzian peak function). Nitrogen sorption measurements were recorded on a Quantachrome Nova 2000 and a Quantachrome Nova 4000e at 77 K. Before the physisorption measurement all samples were outgassed at 423 K overnight under vacuum. Transmission electron microscopic (TEM) images were recorded using a TITAN 80–300 microscope operating at 300 kV. The catalytic experiments were performed in a flow type reactor (0.030 g of catalyst) with a mixture of ethyl acetate (0.6 mol%) in air with WHSV—335 $h^{-1}$. Gas chromatographic (GC) analyses were carried out on a Varian 3700 using carbon-based calibration. The samples were pretreated in Ar at 423 K for 1 h and the temperature was raised with a rate of 2 K/min in the range of 423–670 K for the temperature-programmed regime experiments. After reaching 670 K, time on stream experiments were performed for at least 90 min.

## 3. Results and discussion

### 3.1. Powder X-ray diffraction

PXRD was applied for the identification of $SnO_2$ crystalline phases and the determination of mesostructural arrangements. The low-angle X-ray diffraction patterns of all studied samples remain featureless (not shown) indicating the lack of long-range mesoporous arrangement of the $SnO_2$. Usually heating amorphous $SnO_2$ at temperatures above 573 K leads to its crystallization. Therefore reflections of crystalline $SnO_2$ should be present at higher $2\theta$ angles. The half-width of the reflections gives information about the mean crystal size which can be calculated by the Scherrer equation.

PXRD patterns of $SnO_2$ samples prepared from tin(IV) *tert*-butoxide and $SnCl_4$ after various pre-treatments are depicted in Fig. 1. The obtained PXRD pattern (20–45° $2\theta$) shows two discreet *h k l* reflections at 26.6° and 33.9° $2\theta$ typical of cassiterite, belonging to the 1 1 0 and 1 0 1 crystallographic planes [31]. The first reflection was taken into account for calculating the average grain size assuming that all particles can be approximated as spheres [30].

#### 3.1.1. Intermediate samples

A very interesting result was obtained with the sample $A_P$-(DHT)343. It was found that partial crystallization of the $SnO_2$ could be achieved at temperature as low as 343 K during the specific DHT process (Fig. 1A). The obtained XRD pattern is characterized with broad but well-defined reflections that correspond to $SnO_2$ particles with the smallest sizes of 2.2 nm (Table 1). This proves that at these specific conditions (constant humidity and temperature) the increased mobility and hence the higher reactivity of the $SnO_2$ species are beneficial for crystallization processes to take place within the material.

The use of the "step calcination" procedure allows us to track out the relation between the specific surface area and the progress of $SnO_2$ crystallization and particle growth (Table 1). When no DHT precedes the "step calcination", $A_P$-(SC)498 does not show reflections of crystalline tin dioxide and exhibits very high specific surface area (Table 1, Supporting information Fig. S1). This result is an indication that the surfactant is completely removed at temperatures as low as 498 K. Raman data confirm this as the peaks due to the surfactant in the range of 2800–3000 $cm^{-1}$ disappear at temperatures above 473 K (Supporting information Fig. S2). At the same time, this temperature is still low for the $SnO_2$ crystallization. The further increase of the calcination temperature to 573 K leads to sample $A_P$-(SC)573 with very small $SnO_2$ crystalline particles of about 2.6 nm and two times lower specific surface area (Table 1). The low-temperature $SnO_2$ crystallization during DHT favors the growth of the obtained $SnO_2$ crystallites as their size in $A_P$-(DHT + SC)498 surpasses the one for $A_P$-(SC)573 (Table 1, Supporting information Fig. S 1).

The obtained results with the intermediate samples show the possibility for achieving nanosized $SnO_2$ materials with very high specific surface areas and thus reveal their potential application as active catalytic supports for the introduction and very fine dispersion of active components.

#### 3.1.2. Tin oxides from tin(IV) tert-butoxide

All samples calcined above 573 K are completely crystalline with $SnO_2$ particles in the range of 4.2–6.2 nm (Fig. 1A, Table 1). The size of the crystallites increases with both calcination temperature and the use of DHT. The conducted experiments

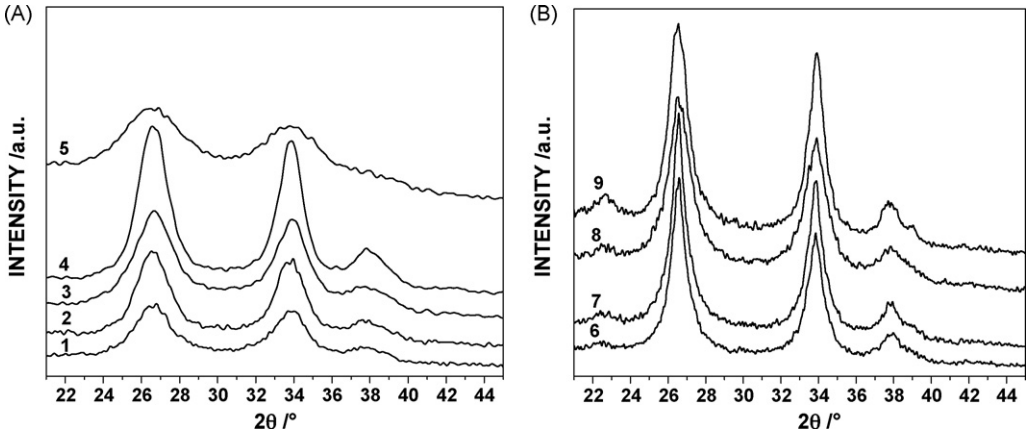


**Fig. 1.** XRD patterns (shifted in *y*-directions) of $SnO_2$ samples prepared from tin(IV) *tert*-butoxide (A): (1) A; (2) A-(DHT); (3) $A_P$; (4) $A_P$-(DHT); (5) $A_P$-(DHT)343 and $SnCl_4$ (B): (6) $B_P$-(DHT); (7) $B_P$; (8) $B_F$ and (9) B.

with the samples containing surfactant and treated with DHT and/or "step calcination" procedures show that the crystallization of the $SnO_2$ species and the growth of the obtained crystallites lead to substantial loss of structural order and hence decrease in the BET surface area and total pore volume (Table 1). One disadvantage of the DHT pre-treatment should not be neglected; the observed particle growth of the cassiterite (up to 30%). Nevertheless, the particle size stays relatively small after calcination at 673 K (Table 1). One way to decrease this particle growth is the combination of both specific treatments (DHT followed by "step calcination") that results in $A_P$-(DHT + SC) with particle sizes smaller than the ones found for $A_P$-(DHT). However, the use of "step calcination" alone results in $A_P$-(SC) with the smallest particle sizes (Table 1).

*3.1.3. Tin oxides from tin chloride.*

In case of the samples obtained with $SnCl_4$, the $SnO_2$ particle size is about two times larger in comparison to tin(IV) *tert*-butoxide samples and depends mainly on the presence or type of surfactant and not on the DHT (Table 1 and Fig. 1B). Here, the smallest particle sizes of about 7 nm were obtained when F127 was used in case of $B_F$ and $B_F$-(DHT). Considerably bigger particles were found when the F127 was replaced with P123 during synthesis (Fig. 1B). The absence of surfactant leads to samples containing $SnO_2$ crystallites with sizes of about 10 nm.

*3.2. Nitrogen physisorption*

Pore properties of the prepared $SnO_2$ powders were characterized by physisorption measurements with nitrogen at 77 K. By recording the adsorption and desorption isotherms, fundamental data including the surface area, pore size distribution and accessible pore volume of the studied materials were obtained (Table 1 and Fig. 2). Fig. 2A–C presents data for the differently prepared $SnO_2$ materials based on Sn(IV) *tert*-butoxide as precursor, and Fig. 2D shows the isotherms for the samples prepared from $SnCl_4$. The obtained isotherms can be classified as type IV isotherms according to IUPAC classification [32]. They are characteristic of mesoporous materials with high energies of adsorption and often contain hysteresis loops attributed to mesoporosity. While it is possible to calculate pore diameters using a model developed by Barret, Joyner and Halenda (BJH) based on the Kelvin equation [33] for pore sizes above seven nm it was shown that the obtained pore sizes are not exact for smaller pores. In our case we used a microscopic model, i.e. the non-local density functional theory NLDFT, which yields more realistic results [34]. Notwithstanding the lack of a perfect match with the real adsorbent situation in the case of the tin dioxide (as the used NLDFT method is adapted strictly to silica) we have obtained good agreement between the theoretical NLDFT isotherm and the

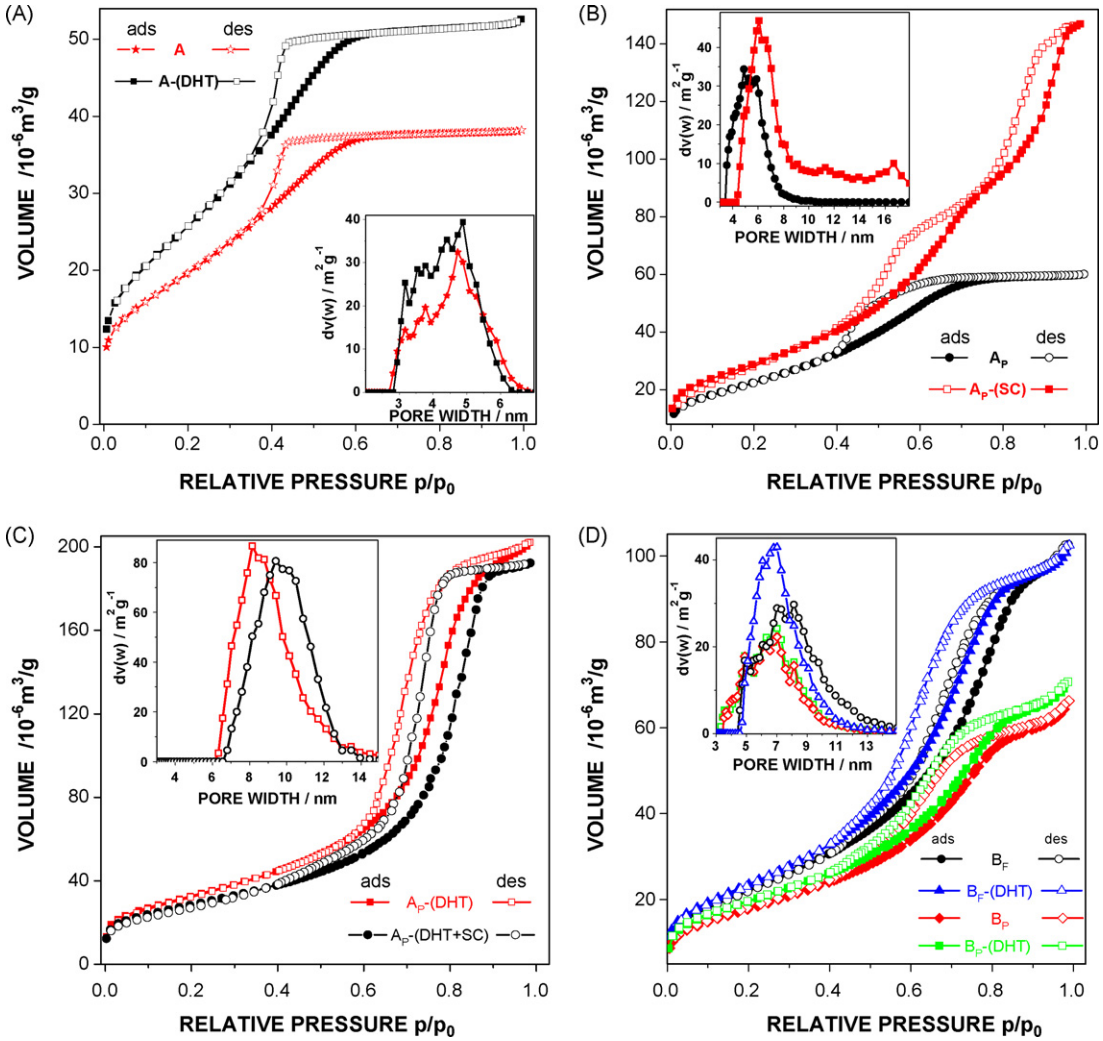


**Fig. 2.** $N_2$ physisorption isotherms of differently treated $SnO_2$ samples prepared from tin(IV) *tert*-butoxide (A–C) and $SnCl_4$ (D). The insets depict the pore size distribution calculated using NLDFT method.

experimental adsorption isotherm as it had previously been reported for other non silicious systems [35].

Samples A and A-(DHT), obtained without structure-director exhibit a type H2 hysteresis loop, which cannot be interpreted easily but most often is related to "ink bottle pores" [34] most probably due to the presence of small inhomogeneous particles. All other investigated samples, but one (sample B, Supporting information Fig. S3) tend to show a type H1 hysteresis usually associated with porous materials consisting of agglomerates of approximately uniform particles or cylindrical mesopores [32,36]. At the same time, in case of sample B the condensation step is observed at very high relative pressures, above 0.9 and the isotherm does not exhibit any limiting adsorption at high partial pressures (Supporting information Fig. S3). This behavior can be assigned to the presence of very large mesopores and macropores are not excluded as well.

The samples prepared without P123 (A and A-(DHT)) exhibit a fairly broad capillary condensation from $p/p_0$ = 0.25–0.55 (Fig. 2A). This observation suggests that the observed pore system is caused by a close packing of small $SnO_2$ particles that are present in these samples. The obtained relatively broad pore size distribution with a median at about 4.5 nm gives rise to a medium specific surface area of 74 $m^2/g$ for sample A. The DHT treatment in this case does not change considerably the profile of the isotherm. For A-(DHT) a substantial increase in the total pore volume and specific surface area is registered which could be an indication of a reorganization of the $SnO_2$ species upon DHT even when no surfactant is present in the system (Table 1 and Fig. 2A).

In case of the samples obtained from tin(IV) *tert*-butoxide with surfactant, an even broader capillary condensation step ($p/p_0$ = 0.25–0.7) is observed (Fig. 2B). We assign this to the presence of surfactant (P123) leading to additional porosity in comparison to A and A-(DHT). The P123 results in additional larger pores upon calcination (Table 1). Here, in comparison to the samples prepared without P123, higher BET surface areas and pore volumes were registered as well. Carrying out the specific pre-treatment like DHT, $A_P$-(DHT), or DHT with addition of "step calcination", $A_P$-(DHT + SC), substantial changes in the shape of the isotherms and the position of the condensation step are observed. After being subjected to DHT, $A_P$-(DHT) is exhibiting a narrower condensation step shifted to higher relative pressures ($p/p_0$ = 0.5–0.85) that we ascribe to the predominant presence of pores referring exclusively to the addition of surfactant (Table 1, Fig. 2C). A change in the obtained isotherms is also found when the step calcination was used alone (sample $A_P$-(SC)). The isotherm of $A_P$-(SC) resembles a mixture of both $A_P$ and $A_P$-(DHT) isotherms (Fig. 2B). Here, two distinct steps in the isotherm were observed that are assigned to the presence of both small and larger mesopores in this sample (Table 1). Besides, the values obtained for the BET surface area and pore volume are inbetween those for $A_P$ and $A_P$-(DHT) as well (Table 1). When DHT is performed before the "step calcination", $A_P$-(DHT + SC), an additional change in the isotherm is observed (Fig. 2C). It is characterized by one condensation step at about 0.8 relative pressures that is an indication of even larger pore sizes compared to $A_P$-(DHT). Furthermore, in comparison with $A_P$-(SC) the total pore volume is much higher, while the BET surface area remains almost constant (Table 1).

In contrast, the use of the specific humidity treatment (DHT) has almost no influence on the pore characteristics of the investigated samples from series B prepared with surfactant (Table 1 and Fig. 2D). Here only a slight increase in the BET surface area is registered for the samples after DHT. It seems that the $SnO_2$ structure is already fixed along the surfactant moieties during the drying step and not as flexible as when we start from the much bulkier Sn(IV) *tert*-butoxide precursor. Both $B_P$ and $B_F$ exhibit isotherms similar to that of sample $A_P$ (Fig. 2A). The use of surfactant with different chain length (P123 or F127) results in samples characterized with different BET surface areas, pore sizes, and total pore volumes (Table 1).

The obtained results from the physisorption measurements show that only when Sn(IV) *tert*-butoxide was used as tin precursor the use of the specific pretreatments has a substantial influence on the final textural characteristics of the $SnO_2$ material in contrast to the reports for the thin films [26,27,37]. The observed change in the position of the condensation step upon addition of surfactant in case of the DHT verifies that a reorganization of the $SnO_2$ species along the surfactant moieties occurs even in powders and is not limited to thin films, i.e. the reorganization proceeds within the bulk of the material as well.

### 3.3. Transmission electron microscopy (TEM)

Fig. 3 presents the TEM (left) and the high resolution TEM (HRTEM) image (right) of $A_P$-(DHT). The TEM image shows a worm-like organization of the $SnO_2$ particles. It seems that the DHT leads eventually to a certain organization of the $SnO_2$ particles along the surfactant used in the synthesis of $A_P$-(DHT) and that suggestion is supported with the considerable increase in specific surface area

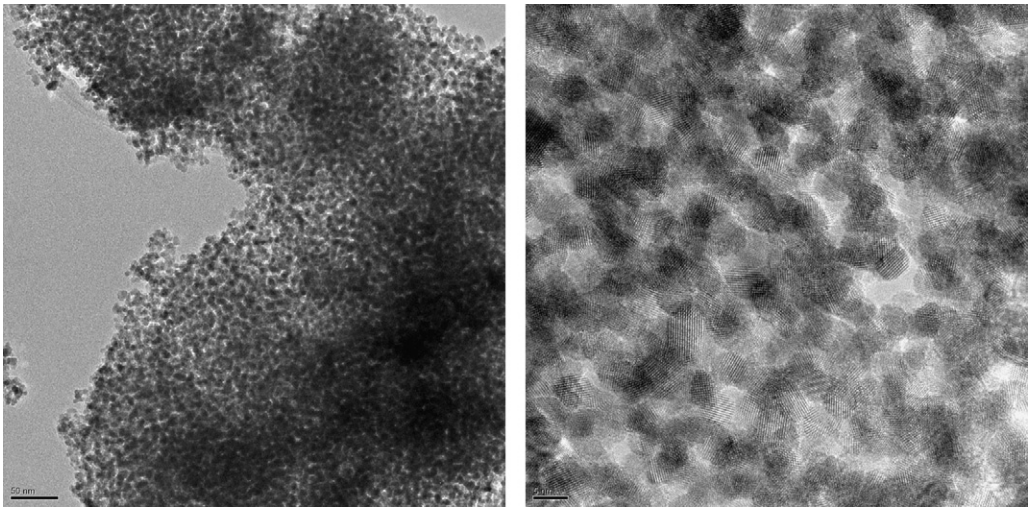


**Fig. 3.** TEM (left) and HRTEM image (right) of $A_P$-(DHT).

and total pore volume in comparison to $A_P$ (Table 1, Fig. 2B and 2C). At the same time, from the HRTEM image (Fig. 3 right) the lattice fringes of the $SnO_2$ particles are clearly visible, confirming the presence of well-crystallized particles with sizes in the range of 5–7 nm in good agreement with the sizes calculated from the XRD data (Table 1).

In our opinion one reason for the stabilization of the particle arrangement could be the process of starting crystallization during the DHT at temperatures as low as 343 K (see sample $A_P$-(DHT)343, Fig. 1A). This low-temperature crystallization seems to stabilize the obtained worm-like ordering for the subsequent calcination.

### 3.4. Catalytic data

In order to study the catalytic behavior of the obtained $SnO_2$ materials in the total oxidation of ethyl acetate we performed experiments with temperature increase as well as with time on stream at a selected temperature (Figs. 4 and 5). All studied $SnO_2$ samples exhibit catalytic activity to ethyl acetate oxidation above 520 K (Fig. 4). At lower conversion rates the main by-products are ethanol and acetaldehyde which are also the typical reaction intermediates. However, above 600 K, these intermediates further oxidize as well and the selectivity towards $CO_2$ increases.

The samples B and $B_F$ obtained from $SnCl_4$ show lower catalytic activity and selectivity to $CO_2$ than the ones prepared with Sn(IV) *tert*-butoxide $A_P$-(SC) and $A_P$ (Figs. 4 and 5). This result could be ascribed not only to the comparatively lower surface areas and larger $SnO_2$ particle sizes but also to the negative impact of residual chloride ions in the system [25].

The additional DHT procedure seems to be beneficial only in case of Sn(IV) *tert*-butoxide samples (Supporting information Fig. S4). This result we ascribe to the higher surface area and the substantially higher pore volume found for A-(DHT) in comparison to A (Table 1, Fig. 2A).

In case of the samples prepared with surfactant the obtained catalytic results for $A_P$-(DHT) (not shown) are very close to those for $A_P$ (Figs. 4 and 5). We explain this with the relatively larger $SnO_2$ particles found for $A_P$-(DHT) that seem to counterbalance the effect of its higher surface area and pore volume. Nevertheless, the higher surface area and pore volume found with the DHT treated samples could be of importance when using these materials as catalytic supports for the introduction of various metals/metal oxides in order to improve their catalytic properties.

In order to study the catalysts stability the samples were subjected to time on stream experiments at 670 K as well (Fig. 5). For all studied samples the reached activity and selectivity values stay stable for at least 90 minutes of the time on stream experiments. The samples arrange in the following order according to their conversion ability and selectivity towards $CO_2$: $A_P$-(SC) > $A_P$-(DHT) ≅ $A_P$ > A-(DHT) > A ≅ B > $B_F$ ≅ $B_F$-(DHT).

In order to find some explanations for the observed catalytic results we show (Fig. 6) the conversion data normalized to the surface area of the studied samples *vs.* temperature (Fig. 6A) and *vs.* time on stream at 670 K (Fig. 6B). The results show that the samples possess uniform active sites. Only in the case of sample B, a certain increase in the number converted ethyl acetate molecules per unit of surface area (respectively per active site) is registered above 600 K and during the time on stream experiments at 670 K (Fig. 6). It is also interesting to stress on the lower selectivity to $CO_2$ which was found for this sample in comparison with the samples prepared with Sn(IV) *tert*-butoxide (Fig. 5). This specific catalytic behavior of sample B we ascribe to its more open pore structure,

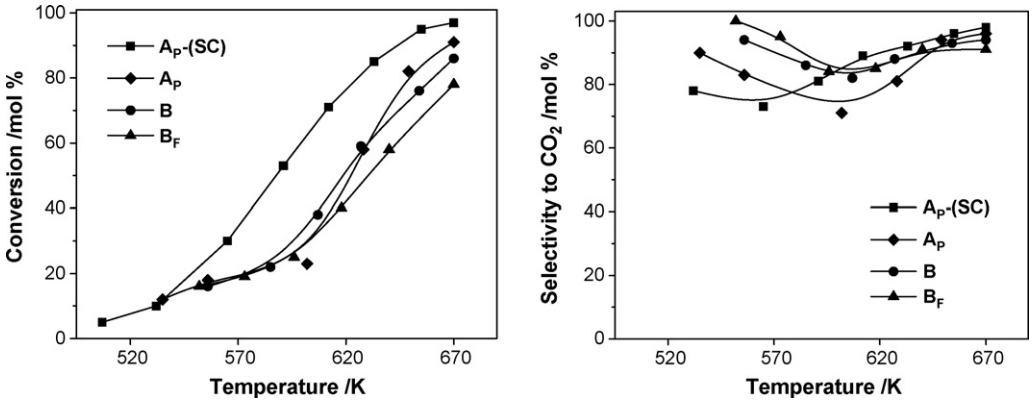


**Fig. 4.** Ethyl acetate conversion *vs.* temperature (left) and selectivity to $CO_2$ *vs.* temperature (right) of differently prepared $SnO_2$ samples.

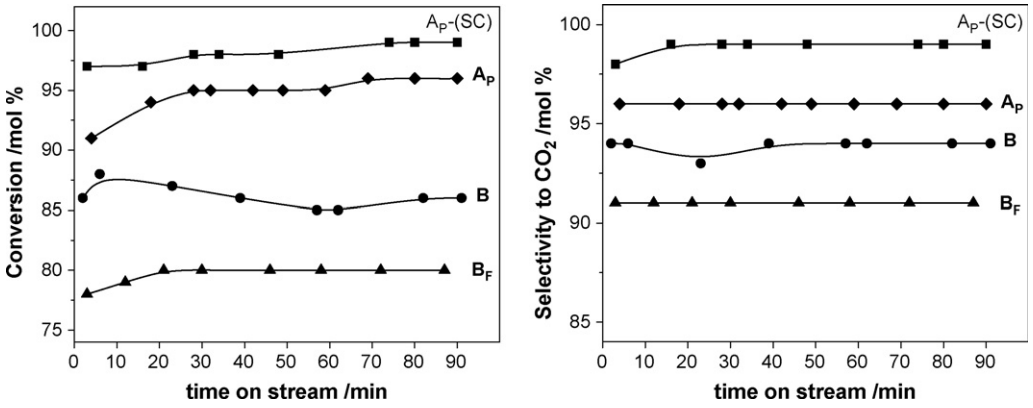


**Fig. 5.** Ethyl acetate conversion (left) and selectivity to $CO_2$ (right) with time on stream at 670 K of differently prepared $SnO_2$ samples.

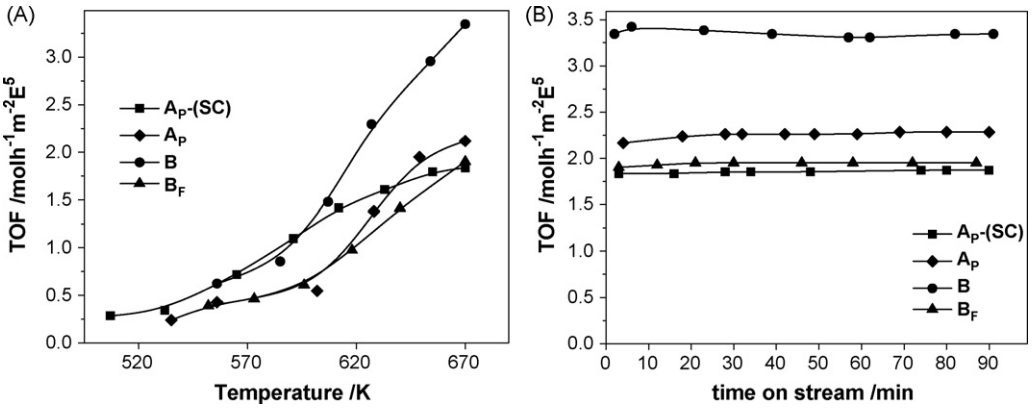


**Fig. 6.** Ethyl acetate conversion normalized to the specific surface area (TOF) *vs.* temperature (A) and *vs.* time on stream at 670 K (B).

characterized with larger meso- and even macropores are not excluded and very high pore volume (Table 1, Fig. S3), which facilitates the mass transport of reagent and intermediates to and from the active sites, respectively. Besides, the lack of sufficient number of active sites due to its lowest surface area is the reason a certain part of the intermediates to leave the catalyst without being further oxidized to $CO_2$ thus transferring them into undesired by-products (Fig. 5).

The best catalytic results were obtained with the sample prepared after using the "step calcination" alone ($A_P$-(SC)). Its conversion curve is shifted at least 30° to lower temperatures (Fig. 4; square symbols) and it shows the highest activity and selectivity to total oxidation of ethyl acetate under isothermal conditions as well (Fig. 5; square symbols). This catalytic behavior could be due to the high specific surface area of the sample, respectively to the high number of catalytic active sites. This high surface area is due predominantly to the smallest particle sizes found for $A_P$-(SC) than to the introduction of surfactant during the synthesis (Table 1). Hence, for this sample a higher exposure of defects is more likely due to the increased surface to volume ratio, which can contribute to the overall number of its active sites. Moreover, in our opinion the presence of these very small particles additionally facilitates the oxygen transfer in the catalyst during the reaction according to the Mars–van Krevelen mechanism [14,15] as well.

This sample seems to have the optimum characteristics needed for this reaction—relatively high BET surface area and pore volume and the smallest particles sizes.

## 4. Conclusions

The influence of specific treatments, calcination procedures, different tin precursors, and surfactants on the textural and catalytic properties of nanocrystalline mesoporous tin dioxide materials have been studied. Thorough characteriation was performed by PXRD, nitrogen physisorption, TEM, and the catalytic total oxidation of ethyl acetate.

Significant textural changes are registered when a specific step calcination procedure and/or a specific delayed humidity treatment DHT are applied. The crystallite size depends on the preparation procedure and the tin precursor. Smaller particles are favored upon step calcination and synthesis from Sn(IV) *tert*-butoxide. They show much higher catalytic activity and selectivity towards $CO_2$. At the same time, the introduction of surfactant leads to higher surface areas and larger pores, while the particles size is almost not affected. The DHT leads to $SnO_2$ crystallization at lower temperature and to a substantial increase in total pore volume and specific surface area which is of importance when aiming for appropriate active catalytic supports.

All investigated samples show catalytic activity in ethyl acetate oxidation and high selectivity towards $CO_2$. This result in combination with their relatively high specific surface areas and pore volumes makes these materials suitable active supports for the introduction of various metals/metal oxides in order to additionally improve their catalytic properties. Further investigations on the physicochemical and catalytic properties of Pd-doped $SnO_2$ catalysts for total oxidation of ethyl acetate are currently in progress.

## Acknowledgements

Financial support by National Science Fund of Bulgaria (Project DO1-907) is gratefully acknowledged. Also the authors would like to thank Shiyu Zhang for the Raman spectra. The authors especially thank Thomas Bein for his constant support.

## Appendix A. Supplementary data

Supplementary data associated with this article can be found, in the online version, at doi:10.1016/j.apcatb.2009.11.004.

## References

[1] G.A. Samorjai, J.Y. Park, Top. Catal. 49 (2008) 126.
[2] B.F.G. Johmson, Top. Catal. 24 (2003) 147.
[3] D.L. Feldheim, Science 316 (2007) 699.
[4] M.-C. Daniel, D. Astruc, Chem. Rev. 104 (2004) 293.
[5] Z.R. Dai, Z.W. Pan, Z.L. Wang, Adv. Funct. Mater. 13 (2003) 9.
[6] L. Vayssieres, A. Hagfeldt, S.E. Lindquist, Pure Appl. Chem. 72 (2000) 47.
[7] G.J. Hutchings, M.S. Scurrell, CATTECH 7 (2003) 90.
[8] M. Skoglundh, A. Ljungqvist, M. Petersson, E. Fridell, N. Cruise, O. Augustsson, E. Jobson, Appl. Catal. B: Environ. 30 (2001) 315.
[9] M. Labaki, J.-F. Lamonier, S. Siffert, E.A. Zhilinskaya, A. Aboukaïs, Kinet. Catal. 45 (2004) 245.
[10] P. Gélin, M. Primet, Appl. Catal. B: Environ. 39 (2002) 1.
[11] H.-G. Lintz, K. Wittstock, Appl. Catal. A: Gen. 216 (2001) 217.
[12] P.-O. Larsson, A. Andersson, Appl. Catal. B: Environ. 24 (2000) 175.
[13] P.-O. Larsson, A. Andersson, J. Catal. 179 (1998) 72.
[14] P. Mars, D.W. van Krevelen, Chem. Eng. Sci. (Special Suppl.) 3 (1954) 41.
[15] C. Doornkamp, V. Ponec, J. Mol. Catal. A: Chem. 162 (2000) 19.
[16] Y. Moro-oka, W. Ueda, K.-H. Lee, J. Mol. Catal. A: Chem. 199 (2003) 139.
[17] A. Taguchi, F. Schüth, Microporous Mesoporous Mater. 77 (2005) 1.
[18] C. Ararat Ibarguen, A. Mosquera, R. Parra, M.S. Castro, J.E. Rodríguez-Páez, Mater. Chem. Phys. 101 (2007) 433.
[19] Ö. Acarbaş, E. Suvac, A. Doğan, Ceram. Int. 33 (2007) 537.
[20] A. Hagemeyer, Z. Hogan, M. Schlichter, B. Smaka, G. Streukens, H. Turner, A. Volpe Jr., H. Weinberg, K. Yaccato, Appl. Catal. A: Gen. 317 (2007) 139.
[21] M. Ristic, M. Ivanda, S. Popovic, S. Music, J. Non-Cryst. Solids 303 (2002) 270.
[22] N.S. Baik, G. Sakai, N. Miura, N. Jamazoe, J. Am. Ceram. Soc. 83 (2000) 2983.
[23] A. Srivastava, S.T. Lakshmikumar, A.K. Srivastava, Rashmi, K. Jain, Sens. Actuators B 126 (2007) 583.
[24] K. Hieda, T. Hyodo, Y. Shimizu, M. Egashira, Sens. Actuators B 133 (2008) 144.
[25] L.B. Fraigi, D.G. Lamas, N.E. Walsöe de Reca, Mater. Lett. 47 (2001) 262.
[26] V.N. Urade, H.W. Hillhouse, J. Phys. Chem. B 109 (2005) 10538.

[27] J.H. Pan, S.Y. Chai, C. Lee, S.-E. Park, W.I. Lee, J. Phys. Chem. C 111 (2007) 5582.
[28] G. De, R. Köhn, G. Xomeritakis, C.J. Brinker, Chem. Commun. (2007) 1840.
[29] V. Beil, Bachelor Thesis, LMU, Munich, 2007.
[30] C. Hammond, The Basics of Crystallography and Diffraction, Oxford Science Publications, New York, 2001, pp. 180–183 (Chapter 9).
[31] W.H. Baur, Acta Crystallogr. 9 (1956) 515.
[32] K.S.W. Sing, D.H. Everett, R.A.W. Haul, L. Moscou, R.A. Pierotti, J. Rouquerol, T. Siemieniewska, Pure Appl. Chem. 57 (1985) 603.
[33] J.B. Condon, Surface Area and Porosity Determinatons by Physisorption—Measurements and Theory, Elsevier, Amsterdam, 2006, p. 21 (Chapter 1).
[34] P.I. Ravikovitch, A.V. Neimark, J. Phys. Chem. B 105 (2001) 6817.
[35] A. Sonnauer, F. Hoffmann, M. Fröba, L. Kienle, V. Duppel, M. Thommes, C. Serre, G. Férey, N. Stock, Angew. Chem. Int. Ed. 21 (2009) 3791.
[36] S. Lowell, J.E. Shields, M.A. Thomas, M. Thommes, Characterization of Porous Solids and Powders: Surface Area, Pore Size and Density, first ed., Kluwer Academic Publishers, Dordrecht, 2004, pp. 43–49 (Chapter 4).
[37] S. Shao, M. Dimitrov, N. Guan, R. Koehn, J. Mater. Chem. 19 (2009) 8411.